

# A Predictive Model of the Temperature-Dependent Inactivation of Coronaviruses

Te Faye Yap,<sup>a</sup> Zhen Liu,<sup>a,†</sup> Rachel A. Shveda,<sup>a,†</sup> Daniel J. Preston<sup>a,\*</sup>

<sup>a</sup>Department of Mechanical Engineering, Rice University, 6100 Main St., Houston, TX 77006

<sup>†</sup>Denotes equal contribution

\*To whom correspondence should be addressed: [djp@rice.edu](mailto:djp@rice.edu)

## ABSTRACT

The COVID-19 pandemic has stressed healthcare systems and supply lines, forcing medical doctors to risk infection by decontaminating and reusing medical personal protective equipment intended only for a single use. The uncertain future of the pandemic is compounded by a lack of data on the ability of the responsible virus, SARS-CoV-2, to survive across various climates, preventing epidemiologists from accurately modeling its spread. However, existing data on the thermal inactivation of related coronaviruses can provide insights enabling progress towards understanding and mitigating COVID-19. This paper describes a thermodynamic model that synthesizes data from the literature to accurately predict the temperature-dependent inactivation of coronaviruses. The model provides much-needed thermal sterilization guidelines for personal protective equipment, including masks, and will also allow epidemiologists to incorporate temperature into models forecasting the spread of coronaviruses across different climates and seasons.

## INTRODUCTION

The COVID-19 pandemic has spread quickly and overwhelmed medical facilities worldwide, often resulting in a lack of intensive care beds and ventilators. These circumstances have forced doctors to decide which patients to provide with life-saving equipment—and which patients to leave without. The shortages have not only affected patients; facing a lack of masks, face shields, gowns, and other typically-disposable personal protective equipment (PPE), medical workers have had to reuse PPE or work without proper protection. As a result, many of them have been infected with SARS-CoV-2, the virus that causes COVID-19, despite the potential for effective sterilization techniques, including dry heat sterilization. Furthermore, as COVID-19 spreads to almost every region of the globe, epidemiologists need to know how long the virus survives in different climates to precisely predict where to focus limited resources, how to model further spread, and how to predict future seasonal flare-ups.

During previous viral outbreaks, regional shortages of personal protective equipment (PPE) led researchers to explore decontamination procedures that might allow PPE to be reused safely.<sup>1,2</sup> Facing an unprecedented nationwide lack of PPE brought on by the COVID-19 pandemic, medical workers have begun implementing these procedures: For example, The University of Nebraska Medical Center in Omaha began attempting in March 2020 to reuse masks after decontamination with ultraviolet (UV) irradiation.<sup>3</sup> However, UV decontamination faces several drawbacks, including an inability to kill viruses trapped within crevices that are not illuminated and a lack of availability in clinics in low-income areas and in most peoples' homes.<sup>4</sup> Other methods of decontamination, namely steam sterilization, alcohol washing, and bleach washing, are useful for items like glassware and other durable materials, but have been reported to degrade surgical masks and other delicate PPE not intended for reuse.<sup>2,5,6</sup> Dry heat sterilization, on the other hand, can be performed almost anywhere (including in home ovens intended for cooking), and viruses inside of crevices or within fabrics are easily inactivated. In addition, while dry heat sterilization is often performed at 160 °C or higher, it can effectively inactivate viruses at much lower temperatures as well (albeit over longer periods of time), enabling sterilization and reuse of delicate PPE

intended for disposal after a single use.<sup>7</sup> However, at this time, appropriate dry heat sterilization guidelines for single-use PPE do not exist.

Meanwhile, virus transmission has been linked to both seasonal and regional variations in climate, where colder atmospheric temperatures typically lead to longer virus lifetimes outside of their hosts. This effect has been reported for both influenza<sup>8,9</sup> and the common cold,<sup>10</sup> and even SARS-CoV-1 has been shown to survive longer at lower temperatures.<sup>11</sup> Epidemiologists require more information on the lifetime of SARS-CoV-2 as a function of atmospheric temperature in order to accurately model the spread of COVID-19. Furthermore, understanding this temperature-dictated inactivation time could help predict whether the autumn and winter will bring a resurgence of cases as the colder weather returns, following a similar trend to that of the seasonal flu.<sup>12</sup>

In this work, we describe a simple model based on the rate law and Arrhenius equation for the thermal inactivation of a range of coronaviruses, essentially treating the viruses as macromolecules that undergo thermal denaturation. Our model predicts the time required to achieve a desired log-scale reduction in viable virions (e.g. by a factor of  $10^6$  as typically used for sterilization<sup>13–16</sup>) at a given temperature. Based on our model, we provide conservative guidelines for dry heat sterilization of coronaviruses that may be used to safely enable sterilization of the SARS-CoV-2 coronavirus at temperatures achievable in commonly available equipment like home-use cooking ovens and rice cookers. We also estimate, based on data for human coronaviruses similar in structure and inactivation behavior<sup>17</sup> to SARS-CoV-2, including SARS-CoV-1, the inactivation rate of human coronaviruses in various climates. We believe these results will be of extreme importance to epidemiologists in predicting the regionally-dependent lifetime of the SARS-CoV-2 virus as well as the severity of the resurgence of COVID-19 that we may face this upcoming autumn and winter.

## RESULTS

Reports in the literature describe the inactivation of many strains of viruses over time, with experiments in different reports conducted over a range of temperatures, providing abundant data upon which a predictive analytical model capturing the influence of thermal effects on virus inactivation may be constructed. In this work, we focused specifically on the inactivation of coronaviruses, a group of enveloped viruses that contain positive sense single-stranded RNA and are often responsible for respiratory or gastrointestinal diseases in mammals and birds.<sup>18</sup> Specifically, we focused on five types of coronaviruses, with subdivisions in data between types of viruses based on (i) strains of each virus, (ii) pH levels, and (iii) relative humidity conditions during experiments, resulting in thirteen sets of data (**Figure 1(a)**). These viruses include: (i) Severe Acute Respiratory Syndrome Coronavirus (SARS CoV-1);<sup>19–21</sup> (ii) Middle East Respiratory Syndrome Coronavirus (MERS-CoV);<sup>22,23</sup> (iii) Transmissible Gastroenteritis Virus (TGEV);<sup>24</sup> (iv) Mouse Hepatitis Virus (MHV);<sup>25,26</sup> and (v) Porcine Epidemic Diarrhea Virus (PEDV).<sup>27</sup> The first two viruses are highly pathogenic human coronaviruses that cause life-threatening respiratory diseases; SARS-CoV-2, the virus responsible for the COVID-19 pandemic, is closely related to SARS-CoV-1 and exhibits many chemical and biological similarities.<sup>28</sup> The latter three viruses are zoonotic viruses known to cause mild to severe illnesses in humans. In each of these studies evaluating thermal inactivation characteristics of coronaviruses, viral inocula were exposed to different temperatures at varying time intervals. Samples were prepared by either suspending the viral stock in an appropriate test tube medium or depositing on a material surface. After exposure to different temperatures, samples on surfaces were recovered to a minimum essential medium. Either a plaque assay or a 50% tissue culture infectious dose (TCID<sub>50</sub>) assay was used to evaluate the infectious titer; we converted TCID<sub>50</sub> results to number of plaque forming units by multiplying by 0.69 based on theory, as performed in prior work.<sup>29–31</sup> Some of these reports also explored on the effects of pH and relative humidity on viral infectivity.<sup>24,27,32</sup>

The inactivation behavior of microbes can be described accurately by the rate law.<sup>33</sup> Non-first-order rate laws have been applied to inactivation of some microbes,<sup>34–36</sup> particularly bacteria with heterogeneous populations,<sup>37</sup> but the inactivation of most viruses—including the viruses considered in our analysis—follows a first-order reaction, with viable virions as products and inactivated virions as reactants (Eq. 1):

$$[C] = [C_0]e^{-kt} \quad (\text{eq. 1})$$

The majority of primary experimental data for the inactivation of viruses is reported in plots of the log of concentration  $\ln([C])$  as a function of time. The rate constant,  $k$ , can be determined from the primary data by fitting a line to data taken at a given temperature,  $T$ , and calculating the slope,  $k = \Delta \ln([C])/\Delta t$ . Each of these pairs of ( $k$ ,  $T$ ) equate to one data point in **Figure 1(a)**. We fitted straight lines to the primary data for each of the viruses studied here; these linear fits are included in the Supporting Information.

Virus inactivation occurs primarily due to thermal denaturation of the proteins that comprise each virion. The temperature dependence of this thermal denaturation process is captured by the Arrhenius relationship,<sup>38</sup> which yields a linear relationship between  $\ln(k)$  and  $1/T$  (Eq. 2):

$$\ln(k) = -E_a/RT + \ln(A) \quad (\text{eq. 2})$$

where  $R$  is the gas constant,  $E_a$  is the activation energy associated with inactivation of the virus (i.e., the energy barrier that must be overcome for protein denaturation), and  $A$  is the frequency factor. Therefore, in **Figure 1(a)**, we applied linear fits to the data to enable continuous prediction of the reaction rates over the full range of temperatures. The activation energy,  $E_a$ , and natural log of the frequency factor,  $\ln(A)$ , were calculated for each virus by equating  $-E_a/R$  and  $\ln(A)$  from Eq. 2 with the slopes and intercepts from the linear fits in **Figure 1(a)**, respectively, and are plotted in **Figure 1(b)**. The correlation between  $\ln(A)$  and  $E_a$  indicates a thermal denaturation process,<sup>39</sup> in agreement with our assertion that the coronaviruses investigated here are inactivated primarily by thermally-driven protein denaturation. In fact, the slope and intercept of a best-fit line applied to the data, for which we calculate  $[\ln(A) = 0.392E_a - 5.43]$  from the dataset used in this work, are nearly identical to the slopes and intercepts of  $[\ln(A) = 0.380E_a - 5.27]$ <sup>39</sup> and  $[\ln(A) = 0.383E_a - 5.95]$ <sup>40</sup> reported in prior work on denaturation of tissues and cells.

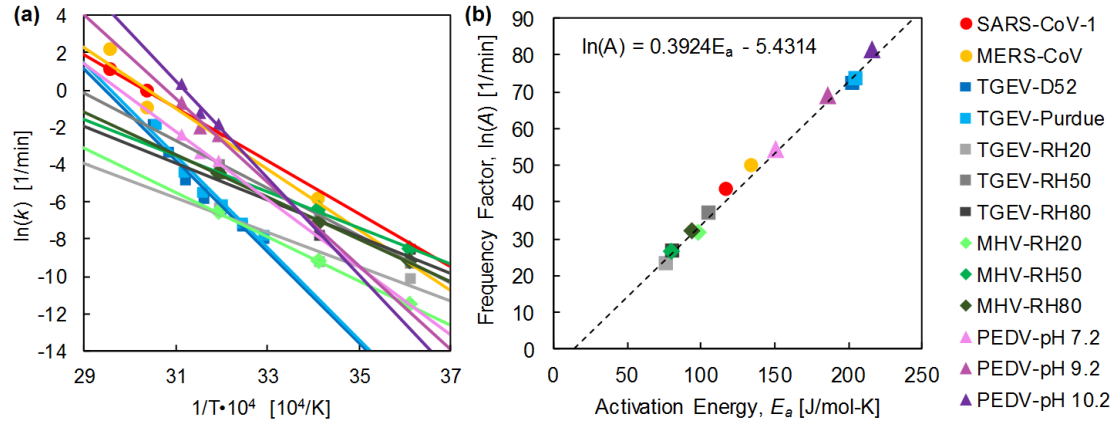


**Figure 1.** Dependence of inactivation rate on temperature, compiled from literature on several strains and under different humidity conditions for SARS-CoV-1, MERS-CoV, TGEV, MHV, and PEDV (a). Each dataset has been fitted with a linear curve according to Eq. 2, and the resulting activation energy and frequency factor were back-calculated from each linear fit according to Eq. 2 and plotted (b); the linear correlation between the log of frequency factor versus activation energy for the set of coronaviruses considered here supports our hypothesis that they are inactivated due to protein denaturation.<sup>39</sup>

The degree of inactivation of a pathogen is defined by the ratio of the concentration (amount) of a pathogen compared to its initial concentration,  $[C]/[C_0]$ , with varying levels of inactivation corresponding to rigor of sterilization reported in the literature, often in terms of orders of magnitude; an  $n$ -log inactivation refers to a reduction in concentration of 10 raised to the  $n$ th power ( $[C]/[C_0] = 10^{-n}$ ). Equations 1 and 2 combine to yield the time required to achieve an  $n$ -log reduction in a pathogen (Eq. 3):

$$t_{n-log} = -\frac{1}{A} e^{\left(\frac{E_a}{RT}\right)} \ln(10^{-n}) \quad (\text{eq. 3})$$

The US Food and Drug Administration recommends a 6-log reduction in concentration of a pathogen (i.e.  $[C]/[C_0] = 10^{-6}$ ) for sterilization.<sup>13-16</sup> We use this value throughout the remainder of our analysis to indicate sterilization times and lifetimes of viruses, although a more conservative value inserted into Eq. 3 would change all of the resulting predictions by a simple multiplicative factor of  $n/6$  (e.g. to achieve a 12-

log reduction in a virus would require doubling all of the times predicted in this work). The predictions generated from Eq. 3 are plotted in **Figure 2** and detailed in **Tables 1** and **2**.

**Figure 2** shows the model predictions of thermal sterilization time as a function of temperature ranging from room temperature to temperatures achievable using common heating devices. In **Figure 2(a)**, all five types of coronaviruses (subdivided according to virus strain and the experimental conditions of relative humidity and pH, as applicable) are plotted to show the variation across different conditions and types of coronavirus. The plot in **Figure 2(b)** shows the same data, with the exception of data sourced from Casanova, et al.,<sup>11</sup> due to potential experimental error (see Supporting Information, Section S3). The same data from **Figure 2(b)** is replotted in **Figure 2(c)** with the sterilization time axis scaled linearly to highlight the exponential dependence on the temperature. **Figure 2(d)** focuses solely on the two human coronaviruses included in this work; SARS-CoV-1 and MERS-CoV exhibit a similar trend in thermal degradation, and recent work has shown that SARS-CoV-2 behaves much like SARS-CoV-1.<sup>17</sup>

The data in **Table 1** summarizes the maximum and average sterilization times required for inactivation of all coronaviruses and the subset of human coronaviruses (SARS-CoV-1 and MERS-CoV) analyzed in this work. The values displayed in the table were selected to demonstrate that thermal sterilization is feasible at relatively low temperatures, albeit requiring longer sterilization times. The maximum coronavirus sterilization time values are extracted from the data in **Figure 2(a)** to provide the most conservative sterilization guidelines by taking the maximum values from predictions incorporating the full data set. The geometric mean was used to calculate the average sterilization time for the same set of data. The data shown in **Figure 2(d)** was used to calculate the maximum temperature for human coronavirus sterilization time, and the geometric mean was used to calculate the average sterilization time. Meanwhile, **Table 2** shows the time required for human coronaviruses to thermally denature outside a host under different environmental temperatures, with the temperature range corresponding to seasonal weather patterns.

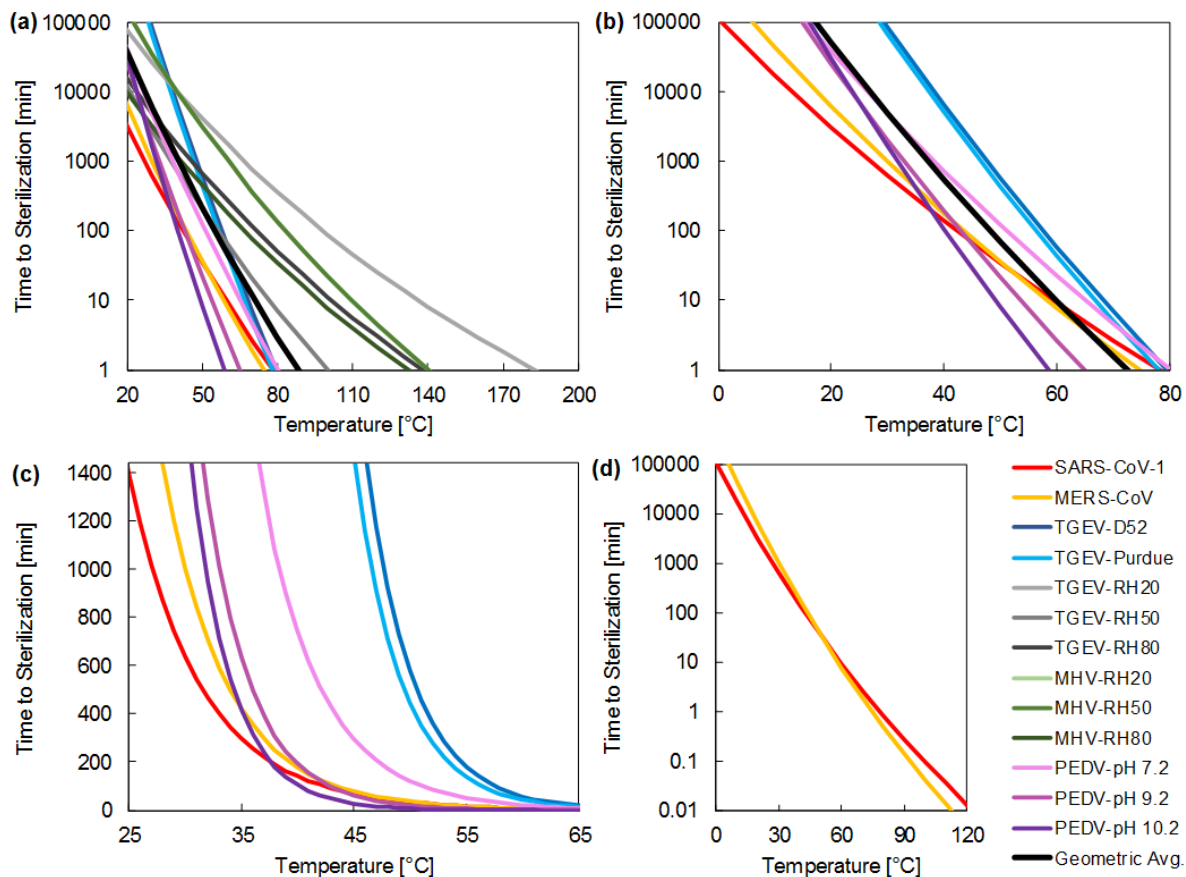


**Figure 2.** Model predictions of the time required for sterilization as a function of temperature for (a) all data analyzed in this work and (b) all data excluding the data from Casanova, et al., where the average curves apply to the data shown in each panel. The subset of data in (b) is replotted with a linearly-scaled vertical axis (1440 minutes = 1 day) to highlight the exponential dependence of sterilization time on temperature (c). The two human coronaviruses included in this work exhibit similar thermal degradation behavior and sterilization times (d).



**Table 1.** Maximum and average sterilization times required for inactivation of all coronaviruses and for the subset of human coronaviruses (SARS-CoV-1 and MERS-CoV) analyzed in this work.

Temperature	Maximum coronavirus sterilization time, $t_{6\text{-log}}$	Average coronavirus sterilization time, $t_{6\text{-log}}$	Max. human coronavirus sterilization time, $t_{6\text{-log}}$	Avg. human coronavirus sterilization time, $t_{6\text{-log}}$
60 °C	29 h	48 min	9 min	8 min
80 °C	6 h	3 min	< 1 min	< 1 min
100 °C	89 min	< 1 min	< 1 min	< 1 min

**Table 2.** Time required for inactivation due to thermal denaturation of human coronaviruses outside of hosts across environmental temperatures ranging from 0 °C to 40 °C.

Temperature	SARS-CoV-1 inactivation time, $t_{6\text{-log}}$	MERS-CoV inactivation time, $t_{6\text{-log}}$
0 °C	> 1 month	> 1 month
5 °C	30.1 d	> 1 month
10 °C	12.2 d	31.1 d
15 °C	5.1 d	11.5 d
20 °C	2.2 d	4.3 d
25 °C	23.3 h	1.7 d
30 °C	10.6 h	16.7 h
35 °C	4.9 h	7.0 h
40 °C	2.4 h	3.0 h

Depending on regional temperatures, coronavirus inactivation times may vary significantly. We estimated the average time required for a 6-log reduction in concentration for SARS-CoV-1 and MERS-CoV, corresponding to the effective lifetime of these viruses, based on regional temperatures in the United States averaged over January to March, 2020, corresponding to the timeline of the COVID-19 pandemic to date. Virus inactivation times were determined using Eq. 3 and the appropriate  $E_a$  and  $\ln(A)$  data. **Figure 3** shows a map of the United States with regions of different average temperatures and the corresponding estimated inactivation time for SARS-CoV-1 and MERS-CoV (details in the Supporting

Information, Section S4). The predictions in **Figure 3** are based on a simplified constant temporal temperature profile and do not account for daily temperature fluctuations, which may result in even shorter inactivation times than predicted due to the exponential dependence of reaction rate on temperature. Additional environmental effects, like UV from sunlight, may further reduce inactivation time; with these limitations in mind, predicted inactivation times longer than one month are not reported.

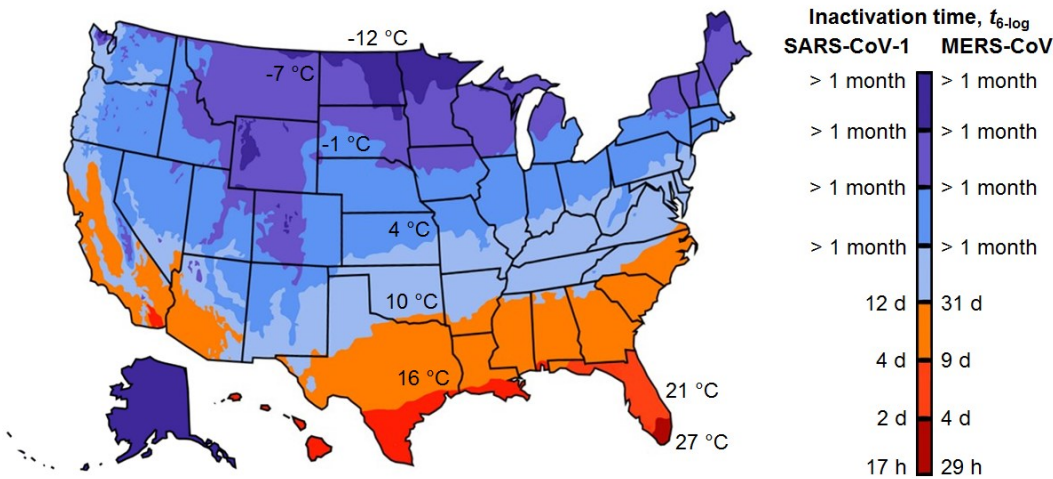


**Figure 3.** Predicted time required for inactivation of SARS-CoV-1 and MERS-CoV outside of a host across the United States based on average temperature data from January to March, 2020.

## DISCUSSION

We compared results from the thermodynamic model presented here with experimental data that had not been used as part of the model training data in order to test its predictive ability. SARS-CoV-1 has been reported to require 22 days at 4 °C to achieve a 4-log reduction, and between 1-2 days at 20 °C to achieve a 5-log reduction; our model predicts times of 24 days and 1.8 days under the same conditions, respectively, in good agreement with the reported data.<sup>41</sup> In another report, SARS-CoV-1 was heated to 56 °C and required only 6 minutes to achieve a 6-log reduction;<sup>20</sup> our model predicts a time of 15 minutes. A third report claimed that SARS-CoV-1 required 30 minutes to achieve an approximately 6-log reduction at 60 °C; our model predicts a time of 9 minutes.<sup>42</sup> Finally, recent work showed that SARS-

CoV-1 underwent a 2-to-3-log reduction over 8 to 24 hours at room temperature;<sup>17</sup> our model predicts a timeframe of 18 to 26 hours. Considering the demonstrated similarity in inactivation behavior of SARS-CoV-1 and SARS-CoV-2,<sup>17</sup> as well as the similarity in our model predictions for different strains of other coronaviruses (**Figure S23**), the model presented here will likely be a useful tool to estimate the thermally-dependent inactivation behavior of SARS-CoV-2 based on predictions for SARS-CoV-1.

This model is limited to temperature-based predictive ability, and does not consider other environmental variables like the relative humidity and the surface material on which a virion rests, both of which appear to have an effect on inactivation times.<sup>11,17,43</sup> Variations in inactivation time at a given temperature due to these environmental factors may be interpreted as catalytic effects,<sup>44</sup> where the activation energy is lowered on solid surfaces, in the presence of water vapor, or even under different pH levels (effect shown in **Figure S26**). Incorporating such an adjustment to the activation energy into the present model would enable, in addition to temperature, predictive capability for other environmental conditions as well. Another limitation of this model is its reliance on a limited set of primary data, which is taken under different conditions and may also contain experimental error (all primary data is shown in the Supporting Information). In addition, although most of the predictive capability of our model is applied within the range of temperatures corresponding to the primary data, the ability of our model to extrapolate to higher temperatures (e.g. above 100 °C) may be unfounded if new inactivation reaction pathways become available at higher temperatures.

Fortunately, the results in **Table 1** indicate that dry heat sterilization is feasible for inactivation of coronaviruses. The most common material used in surgical masks and N95 respirators is non-woven polypropylene.<sup>45,46</sup> Polypropylene is mainly used in room temperature conditions, already well above its glass transition temperature<sup>47,48</sup> and within a region of near-constant stiffness until approaching its melting point, which is typically within the range 156 °C to 168 °C.<sup>49,50</sup> Cui and colleagues suggest that thermal cycling (75 °C, 30 min heating, applied over 20 cycles) does not degrade the filtration efficiency

of N95-level facial masks,<sup>7</sup> and Lin et al. have shown that there is no significant degradation of surgical masks after heating to 160 °C for 3 min.<sup>5</sup> Therefore, we expect that repeated sterilization at lower temperatures will be effective without degrading masks, while also feasible within relatively short times (less than 10 min; **Table 1**) and achievable for the majority of humans with access to home ovens, rice cookers, or similar inexpensive heating devices.

In summary, this work provides guidelines to the public for the effective, safe thermal sterilization of medical PPE, including surgical masks, gowns, and face shields, and even the cloth masks—already popular worldwide—that the CDC has recommended all US citizens wear during the COVID-19 pandemic,<sup>51</sup> especially given the demonstrated similarity between the inactivation behavior SARS-CoV-1 and SARS-CoV-2.<sup>17</sup> In addition, the sensitivity of coronaviruses to environmental temperature variations shown in **Table 2** and **Figure 3** indicates that the thermal inactivation of SARS-CoV-2 must be considered in epidemiological studies predicting its global spread and, potentially, seasonal recurrence.

## ACKNOWLEDGEMENT

We gratefully acknowledge helpful discussions with Dr. Dimithree Kahanda and financial support from Rice University.

## AUTHOR CONTRIBUTIONS

T.F.Y. and D.J.P. compiled and analyzed the data and developed the analytical model. All authors contributed to writing and editing the manuscript. D.J.P. guided the work.

## NOTES

The authors declare no competing financial interest.

## REFERENCES

- (1) Heimbuch, B. K.; Wallace, W. H.; Kinney, K.; Lumley, A. E.; Wu, C. Y.; Woo, M. H.; Wander, J. D. A Pandemic Influenza Preparedness Study: Use of Energetic Methods to Decontaminate Filtering Facepiece Respirators Contaminated with H1N1 Aerosols and Droplets. *Am. J. Infect. Control* **2011**. <https://doi.org/10.1016/j.ajic.2010.07.004>.
- (2) Viscusi, D. J.; King, W. P.; Shaffer, R. E. Effect of Decontamination on the Filtration Efficiency of Two Filtering Facepiece Respirator Models. *J. Int. Soc. Respir. Prot.* **2007**.
- (3) Kolata, G. As Coronavirus Looms, Mask Shortage Gives Rise to Promising Approach. *The New York Times*. **2020**.
- (4) Cramer, A.; Tian, E.; Yu, S. H.; Galanek, M.; Lamere, E.; Li, J.; Gupta, R.; Short, M. P. Disposable N95 Masks Pass Qualitative Fit-Test But Have Decreased Filtration Efficiency after Cobalt-60 Gamma Irradiation. *medRxiv* **2020**. <https://doi.org/10.1101/2020.03.28.20043471>.
- (5) Lin, T. H.; Tang, F. C.; Hung, P. C.; Hua, Z. C.; Lai, C. Y. Relative Survival of Bacillus Subtilis Spores Loaded on Filtering Facepiece Respirators after Five Decontamination Methods. *Indoor Air* **2018**. <https://doi.org/10.1111/ina.12475>.
- (6) Viscusi, D. J.; Bergman, M. S.; Eimer, B. C.; Shaffer, R. E. Evaluation of Five Decontamination Methods for Filtering Facepiece Respirators. *Ann. Occup. Hyg.* **2009**. <https://doi.org/10.1093/annhyg/mep070>.
- (7) Liao, D. L.; Xiao, W.; Yu, X.; Wang, H.; Zhao, D. M.; Wang, D. Q. Can N95 Facial Masks Be Used after Disinfection? And for How Many Times? *Rep. from Collab. Stanford Univ. 4C Air, Inc* **2020**.
- (8) Lowen, A. C.; Steel, J. Roles of Humidity and Temperature in Shaping Influenza Seasonality. *J. Virol.* **2014**. <https://doi.org/10.1128/jvi.03544-13>.
- (9) Petrova, V. N.; Russell, C. A. The Evolution of Seasonal Influenza Viruses. *Nature Reviews Microbiology*. 2018. <https://doi.org/10.1038/nrmicro.2017.118>.
- (10) Ikäheimo, T. M.; Jaakkola, K.; Jokelainen, J.; Saukkoriipi, A.; Roivainen, M.; Juvonen, R.;

- Vainio, O.; Jaakkola, J. J. K. A Decrease in Temperature and Humidity Precedes Human Rhinovirus Infections in a Cold Climate. *Viruses* **2016**. <https://doi.org/10.3390/v8090244>.
- (11) Casanova, L. M.; Jeon, S.; Rutala, W. A.; Weber, D. J.; Sobsey, M. D. Effects of Air Temperature and Relative Humidity on Coronavirus Survival on Surfaces. *Appl. Environ. Microbiol.* **2010**. <https://doi.org/10.1128/AEM.02291-09>.
- (12) Lin, J.; Kang, M.; Zhong, H.; Zhang, X.; Yang, F.; Ni, H.; Huang, P.; Hong, T.; Ke, C.; He, J. Influenza Seasonality and Predominant Subtypes of Influenza Virus in Guangdong, China, 2004-2012. *J. Thorac. Dis.* **2013**. <https://doi.org/10.3978/j.issn.2072-1439.2013.08.09>.
- (13) Ellis, J. L.; Titone, J. C.; Tomasko, D. L.; Annabi, N.; Dehghani, F. Supercritical CO<sub>2</sub> Sterilization of Ultra-High Molecular Weight Polyethylene. *J. Supercrit. Fluids* **2010**. <https://doi.org/10.1016/j.supflu.2010.01.002>.
- (14) Andersen, H. K.; Fiehn, N. E.; Larsen, T. Effect of Steam Sterilization inside the Turbine Chambers of Dental Turbines. *Oral Surg. Oral Med. Oral Pathol. Oral Radiol. Endod.* **1999**. [https://doi.org/10.1016/S1079-2104\(99\)70271-4](https://doi.org/10.1016/S1079-2104(99)70271-4).
- (15) Mastanaiah, N.; Johnson, J. A.; Roy, S. Effect of Dielectric and Liquid on Plasma Sterilization Using Dielectric Barrier Discharge Plasma. *PLoS One* **2013**. <https://doi.org/10.1371/journal.pone.0070840>.
- (16) Rutala, W. A.; Weber, D. J. Low-Temperature Sterilization Technologies: Do We Need to Redefine “Sterilization”? *Infect. Control Hosp. Epidemiol.* **1996**. <https://doi.org/10.2307/30141007>.
- (17) van Doremalen, N.; Bushmaker, T.; Morris, D. H.; Holbrook, M. G.; Gamble, A.; Williamson, B. N.; Tamin, A.; Harcourt, J. L.; Thornburg, N. J.; Gerber, S. I.; Lloyd-Smith, J. O.; de Wit, E.; Munster, V. J. Aerosol and Surface Stability of SARS-CoV-2 as Compared with SARS-CoV-1. *N. Engl. J. Med.* **2020**. <https://doi.org/10.1056/nejmc2004973>.
- (18) Masters, P. S. The Molecular Biology of Coronaviruses. *Advances in Virus Research.* 2006. [https://doi.org/10.1016/S0065-3527\(06\)66005-3](https://doi.org/10.1016/S0065-3527(06)66005-3).

- (19) Darnell, M. E. R.; Taylor, D. R. Evaluation of Inactivation Methods for Severe Acute Respiratory Syndrome Coronavirus in Noncellular Blood Products. *Transfusion* **2006**.  
<https://doi.org/10.1111/j.1537-2995.2006.00976.x>.
- (20) Kariwa, H.; Fujii, N.; Takashima, I. Inactivation of SARS Coronavirus by Means of Povidone-Iodine, Physical Conditions and Chemical Reagents. In *Dermatology*; **2006**.  
<https://doi.org/10.1159/000089211>.
- (21) Rabenau, H. F.; Cinatl, J.; Morgenstern, B.; Bauer, G.; Preiser, W.; Doerr, H. W. Stability and Inactivation of SARS Coronavirus. *Med. Microbiol. Immunol.* **2005**.  
<https://doi.org/10.1007/s00430-004-0219-0>.
- (22) Leclercq, I.; Batéjat, C.; Burguière, A. M.; Manuguerra, J. C. Heat Inactivation of the Middle East Respiratory Syndrome Coronavirus. *Influenza Other Respi. Viruses* **2014**.  
<https://doi.org/10.1111/irv.12261>.
- (23) van Doremalen, N.; Bushmaker, T.; Munster, V. J. Stability of Middle East Respiratory Syndrome Coronavirus (MERS-CoV) under Different Environmental Conditions. *Eurosurveillance* **2013**, *18* (38), 1–4. <https://doi.org/10.2807/1560-7917.ES2013.18.38.20590>.
- (24) Laude, H. Thermal Inactivation Studies of a Coronavirus, Transmissible Gastroenteritis Virus. *J. Gen. Virol.* **1981**. <https://doi.org/10.1099/0022-1317-56-2-235>.
- (25) Lelie, P. N.; Reesink, H. W.; Lucas, C. J. Inactivation of 12 Viruses by Heating Steps Applied during Manufacture of a Hepatitis B Vaccine. *J. Med. Virol.* **1987**.  
<https://doi.org/10.1002/jmv.1890230313>.
- (26) Saknimit, M.; Inatsuki, I.; Sugiyama, Y.; Yagami, K. Virucidal Efficacy of Physico-Chemical Treatments against Coronaviruses and Parvoviruses of Laboratory Animals. *Jikken Dobutsu.* **1988**.  
[https://doi.org/10.1538/expanim1978.37.3\\_341](https://doi.org/10.1538/expanim1978.37.3_341).
- (27) Quist-Rybachuk, G. V.; Nauwynck, H. J.; Kalmar, I. D. Sensitivity of Porcine Epidemic Diarrhea Virus (PEDV) to PH and Heat Treatment in the Presence or Absence of Porcine Plasma. *Vet. Microbiol.* **2015**. <https://doi.org/10.1016/j.vetmic.2015.10.010>.

- (28) Xu, J.; Zhao, S.; Teng, T.; Abdalla, A. E.; Zhu, W.; Xie, L.; Wang, Y.; Guo, X. Systematic Comparison of Two Animal-to-Human Transmitted Human Coronaviruses: SARS-CoV-2 and SARS-CoV. *Viruses* **2020**. <https://doi.org/10.3390/v12020244>.
- (29) Possee, R. D. Baculovirus Expression Vectors — A Laboratory Manual. *Trends Biotechnol.* **1993**. [https://doi.org/10.1016/0167-7799\(93\)90146-z](https://doi.org/10.1016/0167-7799(93)90146-z).
- (30) Neill, K. O.; Huang, N.; Unis, D.; Clem, R. J. Rapid Selection against Arbovirus-Induced Apoptosis during Infection of a Mosquito Vector. *Proc. Natl. Acad. Sci. U. S. A.* **2015**. <https://doi.org/10.1073/pnas.1424469112>.
- (31) Li, S.; Zhao, H.; Yang, H.; Hou, W.; Cruz-Cosme, R.; Cao, R.; Chen, C.; Wang, W.; Xu, L.; Zhang, J.; Zhong, W.; Xia, N.; Tang, Q.; Cheng, T. Rapid Neutralization Testing System for Zika Virus Based on an Enzyme-Linked Immunospot Assay. *ACS Infect. Dis.* **2020**. <https://doi.org/10.1021/acsinfecdis.9b00333>.
- (32) Hulst, M. M.; Heres, L.; Hakze-van der Honing, R. W.; Pelsler, M.; Fox, M.; van der Poel, W. H. M. Study on Inactivation of Porcine Epidemic Diarrhoea Virus, Porcine Sapelovirus 1 and Adenovirus in the Production and Storage of Laboratory Spray-Dried Porcine Plasma. *J. Appl. Microbiol.* **2019**. <https://doi.org/10.1111/jam.14235>.
- (33) C.R., S. Thermobacteriology in Food Processing (2nd Ed). *New York Acad. Press* **1973**.
- (34) Xiong, R.; Xie, G.; Edmondson, A. E.; Sheard, M. A. A Mathematical Model for Bacterial Inactivation. *Int. J. Food Microbiol.* **1999**. [https://doi.org/10.1016/S0168-1605\(98\)00172-X](https://doi.org/10.1016/S0168-1605(98)00172-X).
- (35) CERF, O. A REVIEW Tailing of Survival Curves of Bacterial Spores. *J. Appl. Bacteriol.* **1977**. <https://doi.org/10.1111/j.1365-2672.1977.tb00665.x>.
- (36) Casolari, A. Microbial Death. In *Physiological Models in Microbiology: Volume II*; **2018**. <https://doi.org/10.1201/9781351075640>.
- (37) Van Boekel, M. A. J. S. On the Use of the Weibull Model to Describe Thermal Inactivation of Microbial Vegetative Cells. *Int. J. Food Microbiol.* **2002**. [https://doi.org/10.1016/S0168-1605\(01\)00742-5](https://doi.org/10.1016/S0168-1605(01)00742-5).



- 364 (38) Price, W. C. Thermal Inactivation Rates of Four Plant Viruses. *Arch. Gesamte Virusforsch.* **1940**.  
 365 <https://doi.org/10.1007/BF01245548>.
- 366 (39) Qin, Z.; Balasubramanian, S. K.; Wolkers, W. F.; Pearce, J. A.; Bischof, J. C. Correlated  
 367 Parameter Fit of Arrhenius Model for Thermal Denaturation of Proteins and Cells. *Ann. Biomed.*  
 368 *Eng.* **2014**. <https://doi.org/10.1007/s10439-014-1100-y>.
- 369 (40) Wright, N. T. On a Relationship between the Arrhenius Parameters from Thermal Damage  
 370 Studies. *J. Biomech. Eng.* **2003**. <https://doi.org/10.1115/1.1553974>.
- 371 (41) Lai, M. Y. Y.; Cheng, P. K. C.; Lim, W. W. L. Survival of Severe Acute Respiratory Syndrome  
 372 Coronavirus. *Clin. Infect. Dis.* **2005**. <https://doi.org/10.1086/433186>.
- 373 (42) Yunoki, M.; Urayama, T.; Yamamoto, I.; Abe, S.; Ikuta, K. Heat Sensitivity of a SARS-  
 374 Associated Coronavirus Introduced into Plasma Products. *Vox Sang.* **2004**.  
 375 <https://doi.org/10.1111/j.1423-0410.2004.00577.x>.
- 376 (43) Chan, K. H.; Peiris, J. S. M.; Lam, S. Y.; Poon, L. L. M.; Yuen, K. Y.; Seto, W. H. The Effects of  
 377 Temperature and Relative Humidity on the Viability of the SARS Coronavirus. *Adv. Virol.* **2011**.  
 378 <https://doi.org/10.1155/2011/734690>.
- 379 (44) Roduner, E. Understanding Catalysis. *Chemical Society Reviews.* **2014**.  
 380 <https://doi.org/10.1039/c4cs00210e>.
- 381 (45) Bałazy, A.; Toivola, M.; Adhikari, A.; Sivasubramani, S. K.; Reponen, T.; Grinshpun, S. A. Do  
 382 N95 Respirators Provide 95% Protection Level against Airborne Viruses, and How Adequate Are  
 383 Surgical Masks? *Am. J. Infect. Control* **2006**, 34 (2), 51–57.  
 384 <https://doi.org/10.1016/j.ajic.2005.08.018>.
- 385 (46) Belkin, N. L. The Surgical Mask: Are New Tests Relevant for OR Practice? *AORN J.* **2009**, 89 (5),  
 386 883–891. <https://doi.org/10.1016/j.aorn.2008.09.016>.
- 387 (47) Passaglia, E.; Martin, G. M. Variation of Glass Temperature with Pressure in Polypropylene. *J.*  
 388 *Res. Natl. Bur. Stand. Sect. A Phys. Chem.* **1964**, 68A (3), 273.  
 389 <https://doi.org/10.6028/jres.068a.024>.

- (48) Bu, H.-S.; Cheng, S.; Wunderlich, B. Addendum to the Thermal Properties of Polypropylene. *Die Makromol. Chemie, Rapid Commun.* **1988**, *9* (2), 75–77.  
<https://doi.org/10.1002/marc.1988.030090205>.
- (49) Tiganis, B. E.; Shanks, R. A.; Long, Y. Effects of Processing on the Microstructure, Melting Behavior, and Equilibrium Melting Temperature of Polypropylene. *J. Appl. Polym. Sci.* **1996**, *59* (4), 663–671. [https://doi.org/10.1002/\(sici\)1097-4628\(19960124\)59:4<663::aid-app12>3.3.co;2-c](https://doi.org/10.1002/(sici)1097-4628(19960124)59:4<663::aid-app12>3.3.co;2-c).
- (50) Duran, K.; Duran, D.; Oymak, G.; Kiliç, K.; Öncü, E.; Kara, M. Investigation of the Physical Properties of Meltblown Nonwovens for Air Filtration. *Tekst. ve Konfeksiyon* **2013**, *23* (2), 136–142.
- (51) Michael D. Shear; Sheila Kaplan. A Debate Over Masks Uncovers Deep White House Divisions. *The New York Times*. **2002**.

## SUPPORTING INFORMATION FOR:

### A Predictive Model of the Temperature-Dependent Inactivation of Coronaviruses

Te Faye Yap,<sup>a</sup> Zhen Liu,<sup>a,†</sup> Rachel A. Shveda,<sup>a,†</sup> Daniel J. Preston<sup>a,\*</sup>

<sup>a</sup>Department of Mechanical Engineering, Rice University, 6100 Main St., Houston, TX 77006

<sup>†</sup>Denotes equal contribution;

\*To whom correspondence should be addressed: [djp@rice.edu](mailto:djp@rice.edu)

#### **Table of Contents**

#### **S1. Homogenization of Virus Inactivation Data**

#### **S2. Processing of Virus Inactivation Data**

#### **S3. Trends Across pH and Relative Humidity**

#### **S4. Conversion of Climate Data to Inactivation Timescale Map**

#### **S1. Homogenization of Virus Inactivation Data**

Data were obtained from the literature and homogenized according to the following procedures: (i) units were converted to standard SI, except for the use of minutes in place of seconds following the convention used in virology; (ii) 50% tissue culture infectious dose (TCID<sub>50</sub>) assay results were converted to number of plaque forming units (PFU) by multiplying by 0.69 based on theory, as performed in prior work;<sup>29–31</sup> (iii) logarithms were all converted to base-*e* (the natural logarithm); (iv) data for which the experimental error bars overlapped the lower detection limit (LDL) of the experimental technique were excluded because they would artificially skew the resulting curve fits towards lower rate constants (i.e. slopes).

### **Data for SARS-CoV-1**

A 50% tissue culture infectious dose (TCID<sub>50</sub>) assay was reported in the work by Darnell, et al. We converted the TCID<sub>50</sub> results to number of plaque forming units (PFU) by multiplying by 0.69 based on theory, as performed in prior work,<sup>29–31</sup> and then converted the data from log<sub>10</sub> to the natural log before plotting against time and taking a linear fit. Data near the lower detection limit (LDL) were excluded from the analysis to avoid under-predicting the rate. In addition, data at 75 °C were excluded because only one data point was not near the LDL, meaning a line could not be fit to the data. Linear fits for the data at 56 °C and 65 °C are presented in **Figures S1** and **S2**. The resulting slopes were used to determine the rate constants at these temperatures, reported in **Table S1**.

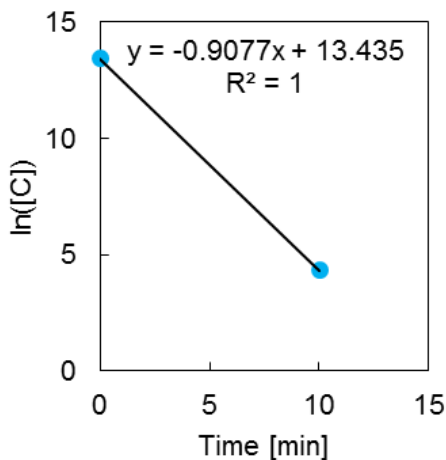


**Figure S1.** Primary data from Darnell, et al.,<sup>19</sup> for inactivation of SARS-CoV-1 at 56 °C after converting the y-values from TCID<sub>50</sub> to PFU and from log<sub>10</sub> to the natural log. We fit a line to the data to determine the rate constant at 56 °C.

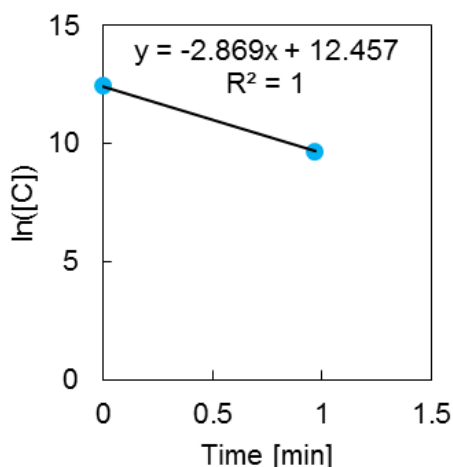


**Figure S2.** Primary data from Darnell, et al.,<sup>19</sup> for inactivation of SARS-CoV-1 at 65°C after converting the y-values from TCID<sub>50</sub> to PFU and from log<sub>10</sub> to the natural log. We fit a line to the data to determine the rate constant at 65 °C.

#### ***Data for MERS-CoV***

A 50% tissue culture infectious dose (TCID<sub>50</sub>) assay was reported in the work by Leclercq, et al. A table with information of the slopes (rate constant) at 56 °C and 65°C was provided. We converted the value of the slopes from log<sub>10</sub> to the natural log and also the TCID<sub>50</sub> results to number of plaque forming units (PFU) by multiplying by 0.69 based on theory, as performed in prior work.<sup>29–31</sup> Data at 25°C were excluded due to the non-physical positive value for the slope (the concentration should decrease with time), which was likely due to experimental error in the measurements eclipsing the small change in concentration at 25°C. The authors also mentioned in the paper that there was no decrease in titre after 2 hours for the data taken at 25°C. The data for 20°C was obtained from work by Doremalen, et al. A TCID<sub>50</sub> assay was reported in their work. We converted TCID<sub>50</sub> results to number of plaque forming units (PFU) by multiplying by 0.69 based on theory, as performed in prior work,<sup>29–31</sup> and then converted the data from log<sub>10</sub> to the natural log before plotting against time and taking a linear fit. A linear fit for the data at 20°C is presented in **Figure S3** and the slope is computed to determine the rate constant at this temperature, reported in **Table S1**.

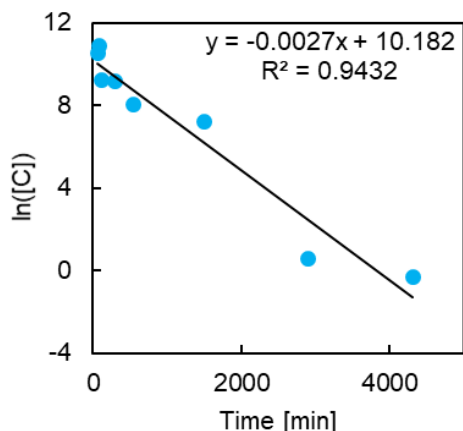


**Figure S3.** Primary data from Doremalen, et al.,<sup>23</sup> for inactivation of MERS-CoV at 20 °C after converting the y-values from TCID<sub>50</sub> to PFU and from log<sub>10</sub> to the natural log. We fit a line to the data to determine the rate constant at 20 °C.

#### ***Data for TGEV-D52 and TGEV-Purdue***

An Arrhenius plot for thermal inactivation of TGEV D52 strain and Purdue strain was reported in the work by Laude, et al. The logarithms of the rate constants were provided for temperatures of 31, 35, 39, 43, 47, 51, and 55 °C. We converted the value of the rate constants from log<sub>10</sub> to the natural log and also converted the units from inverse seconds to inverse minutes to maintain consistency with the other data values used in this work. The converted rate constants are reported in **Table S1**.

#### ***Data for TGEV at relative humidity (RH) values of 20%, 50%, and 80%***

The virus concentration versus time for relative humidity (RH) values of 20%, 50%, and 80% at temperatures of 4, 20, and 40°C was reported in the work by Casanova, et al.<sup>11</sup> We converted the value of the slopes from log<sub>10</sub> to the natural log before plotting against time and taking the linear fit to find the rate constant. Data near the lower detection limit (LDL) were excluded from the analysis to avoid under-predicting the rate (because the slope of the linear fit would artificially become shallower due to the inability to resolve lower concentrations experimentally). Linear fits for the data at 4, 20, and 40 °C and

at relative humidity values of 20%, 50%, and 80%, respectively, are shown in **Figures S4 to S12**. The resulting slopes were used to determine the rate constants at these temperatures, reported in **Table S1**.

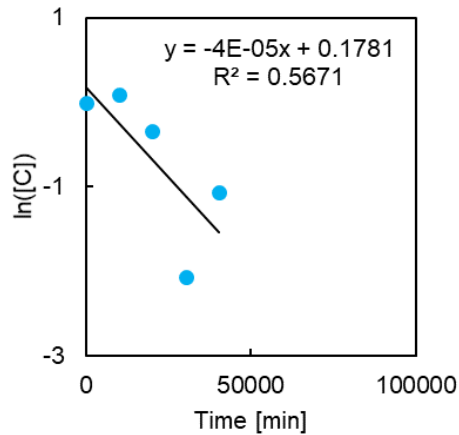


**Figure S4.** Primary data from Casanova et al.,<sup>11</sup> for inactivation of TGEV at 4 °C and relative humidity of 20% after converting the y-values from  $\log_{10}$  to the natural log. We fit a line to the data to determine the rate constant at 4 °C and RH of 20%.

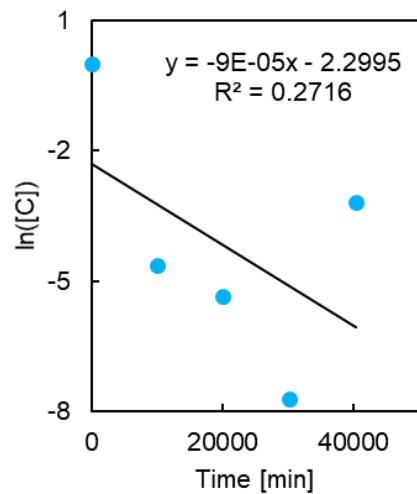


**Figure S5.** Primary data from Casanova et al.,<sup>11</sup> for inactivation of TGEV at 4 °C and relative humidity of 50% after converting values from  $\log_{10}$  to the natural log. We fit a line to the data to determine the rate constant at 4 °C and RH of 50%.

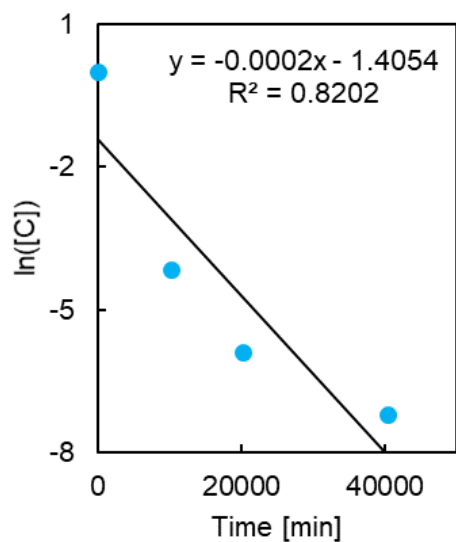


**Figure S6.** Primary data from Casanova et al.,<sup>11</sup> for inactivation of TGEV at 4 °C and relative humidity of 80% after converting values from  $\log_{10}$  to the natural log. We fit a line to the data to determine the rate constant at 4 °C and RH of 80%.

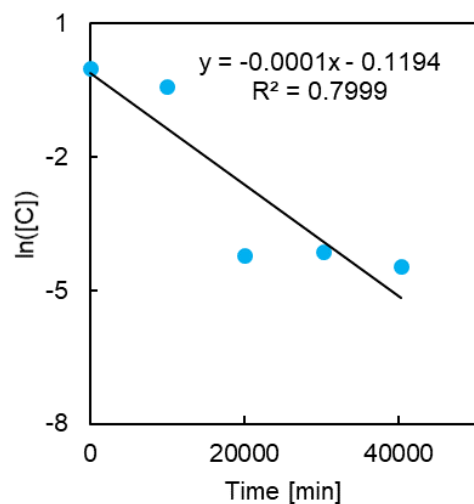


**Figure S7.** Primary data from Casanova et al.,<sup>11</sup> for inactivation of TGEV at 20 °C and relative humidity of 20% after converting values from  $\log_{10}$  to the natural log. We fit a line to the data to determine the rate constant at 20 °C and RH of 20%.



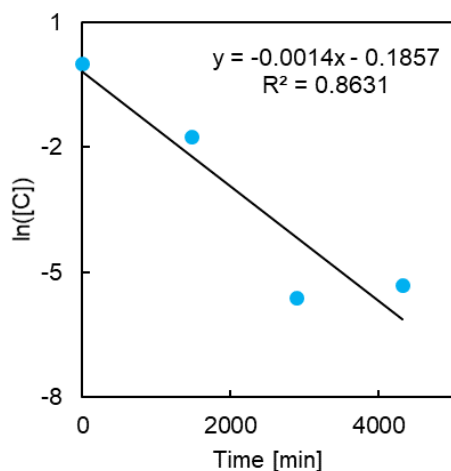


**Figure S8.** Primary data from Casanova et al.,<sup>11</sup> for inactivation of TGEV at 20 °C and relative humidity of 50% after converting values from  $\log_{10}$  to the natural log. We fit a line to the data to determine the rate constant at 20 °C and RH of 50%.

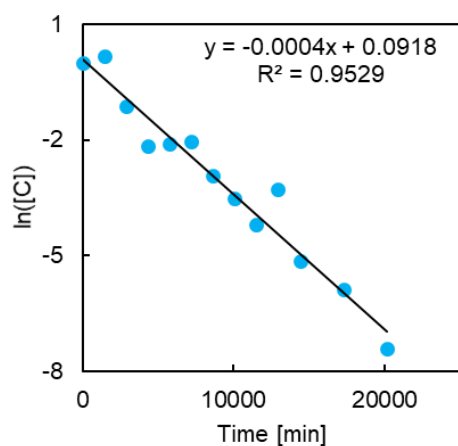


**Figure S9.** Primary data from Casanova et al.,<sup>11</sup> for inactivation of TGEV at 20 °C and relative humidity of 80% after converting values from  $\log_{10}$  to the natural log. We fit a line to the data to determine the rate constant at 20 °C and RH of 80%.

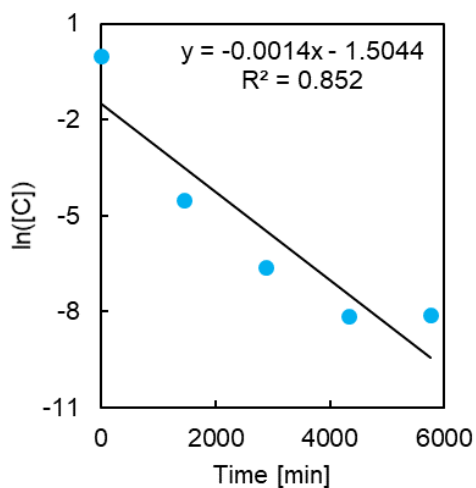


**Figure S10.** Primary data from Casanova et al.,<sup>11</sup> for inactivation of TGEV at 40 °C and relative humidity of 20% after converting values from  $\log_{10}$  to the natural log. We fit a line to the data to determine the rate constant at 40 °C and RH of 20%.

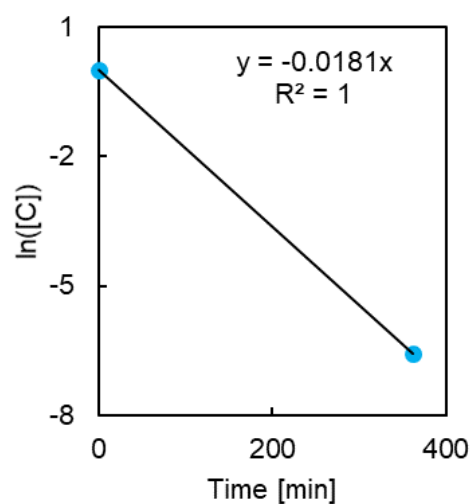


**Figure S11.** Primary data from Casanova et al.,<sup>11</sup> for inactivation of TGEV at 40 °C and relative humidity of 50% after converting values from  $\log_{10}$  to the natural log. We fit a line to the data to determine the rate constant at 40 °C and RH of 50%.

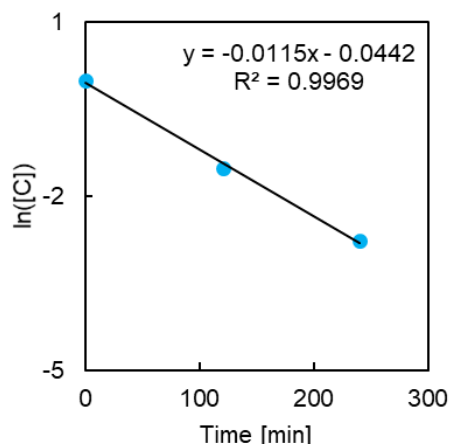


**Figure S12.** Primary data from Casanova et al.,<sup>11</sup> for inactivation of TGEV at 40 °C and relative humidity of 80% after converting values from  $\log_{10}$  to the natural log. We fit a line to the data to determine the rate constant at 40 °C and RH of 80%.

***Data for MHV at relative humidity (RH) values of 20%, 50%, and 80%***

The virus concentration versus time for relative humidity (RH) values of 20%, 50%, and 80% at temperatures of 4, 20, and 40°C was reported in the work by Casanova, et al.<sup>11</sup> We converted the value of the slopes from  $\log_{10}$  to the natural log before plotting against time and taking the linear fit to find the rate constant. Data near the lower detection limit (LDL) were excluded from the analysis to avoid under-predicting the rate (because the slope of the linear fit would artificially become shallower due to the inability to resolve lower concentrations experimentally). Linear fits for the data at 4, 20, and 40°C and at relative humidity values of 20%, 50%, and 80%, respectively, are shown in **Figures S13 to S21**. The resulting slopes were used to determine the rate constants at these temperatures, reported in **Table S1**.

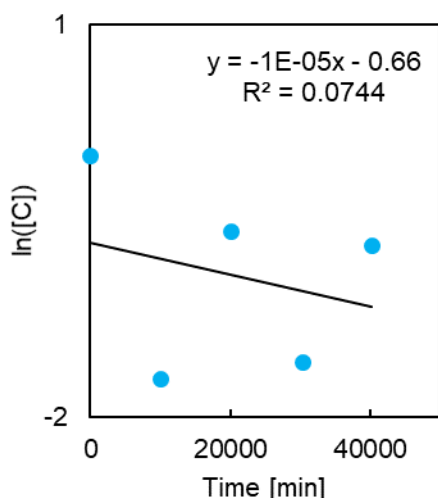


**Figure S13.** Primary data from Casanova et al.,<sup>11</sup> for inactivation of MHV at 4 °C and relative humidity of 20% after converting values from  $\log_{10}$  to the natural log. We fit a line to the data to determine the rate constant at 4 °C and RH of 20%.

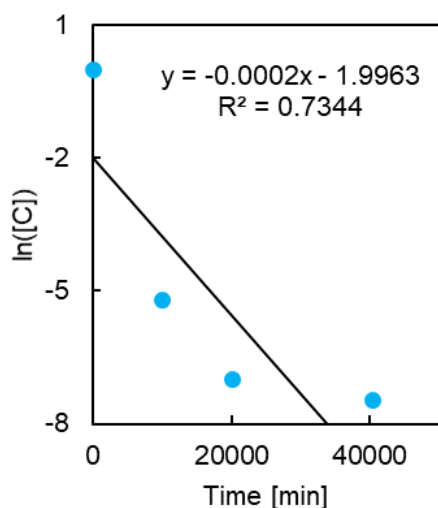


**Figure S14.** Primary data from Casanova et al.,<sup>11</sup> for inactivation of MHV at 4 °C and relative humidity of 50% after converting values from  $\log_{10}$  to the natural log. We fit a line to the data to determine the rate constant at 4 °C and RH of 50%.

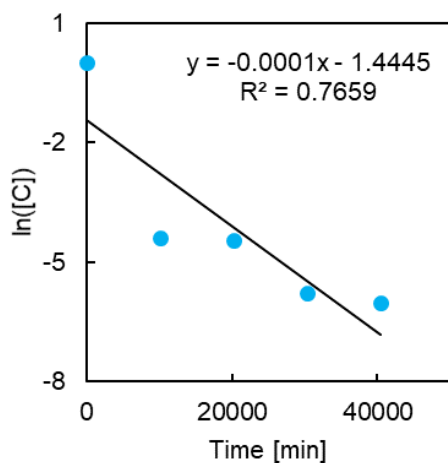


**Figure S15.** Primary data from Casanova et al.,<sup>11</sup> for inactivation of MHV at 4 °C and relative humidity of 80% after converting values from  $\log_{10}$  to the natural log. We fit a line to the data to determine the rate constant at 4 °C and RH of 80%.

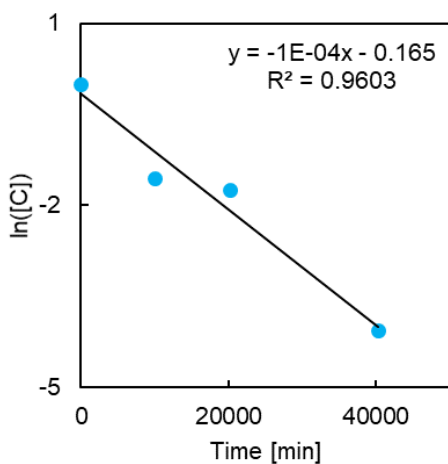


**Figure S16.** Primary data from Casanova et al.,<sup>11</sup> for inactivation of MHV at 20 °C and relative humidity of 20% after converting values from  $\log_{10}$  to the natural log. We fit a line to the data to determine the rate constant at 20 °C and RH of 20%.

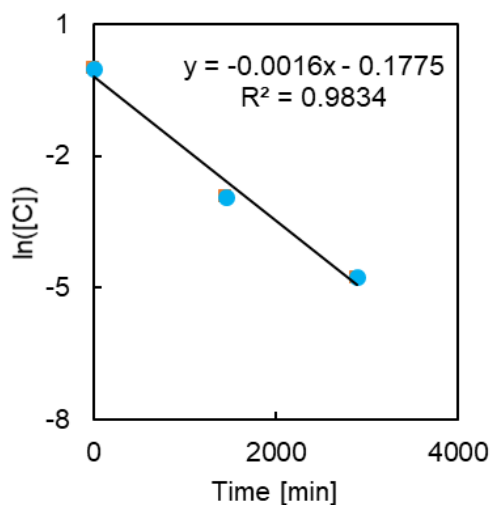


**Figure S17.** Primary data from Casanova et al.,<sup>11</sup> for inactivation of MHV at 20 °C and relative humidity of 50% after converting values from  $\log_{10}$  to the natural log. We fit a line to the data to determine the rate constant at 20 °C and RH of 50%.

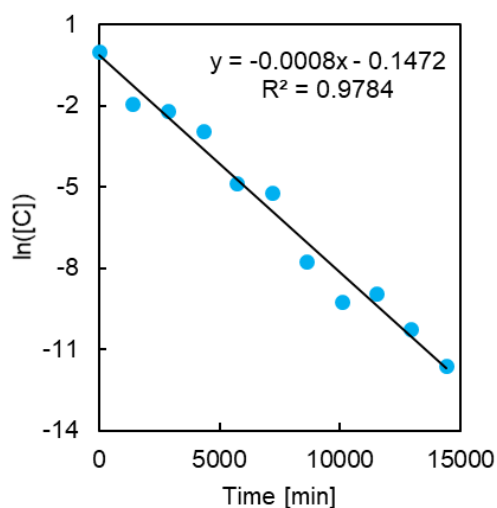


**Figure S18.** Primary data from Casanova et al.,<sup>11</sup> for inactivation of MHV at 20 °C and relative humidity of 80% after converting values from  $\log_{10}$  to the natural log. We fit a line to the data to determine the rate constant at 20 °C and RH of 80%.

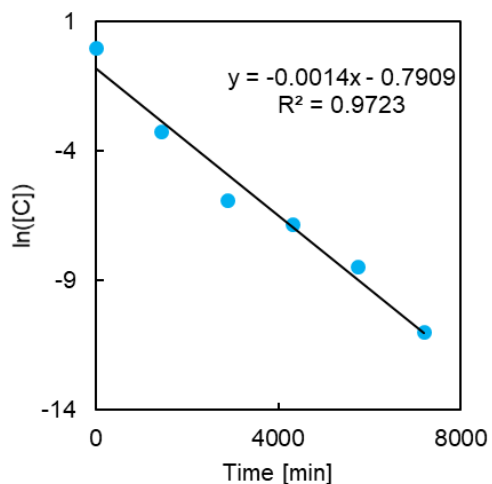


**Figure S19.** Primary data from Casanova et al.,<sup>11</sup> for inactivation of MHV at 40 °C and relative humidity of 20% after converting values from  $\log_{10}$  to the natural log. We fit a line to the data to determine the rate constant at 40 °C and RH of 20%.

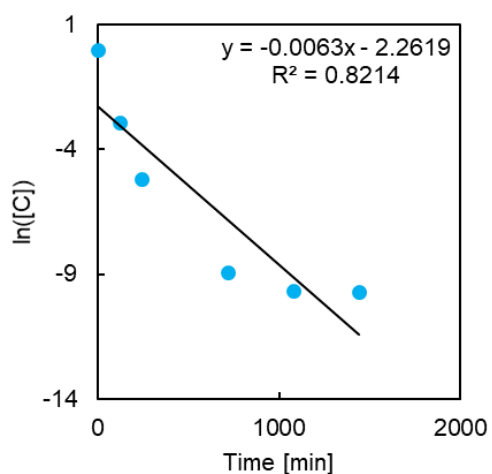


**Figure S20.** Primary data from Casanova et al.,<sup>11</sup> for inactivation of MHV at 40 °C and relative humidity of 50% after converting values from  $\log_{10}$  to the natural log. We fit a line to the data to determine the rate constant at 40 °C and RH of 50%.

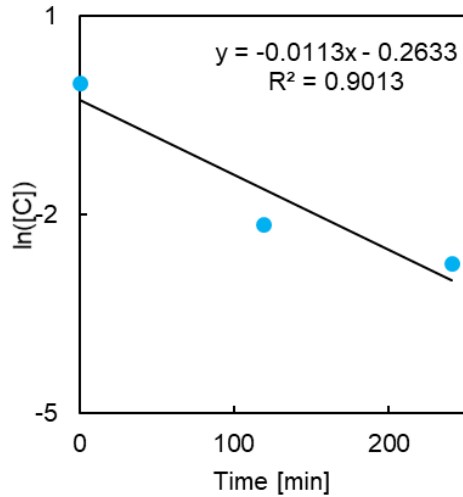


**Figure S21.** Primary data from Casanova et al.,<sup>11</sup> for inactivation of MHV at 40 °C and relative humidity of 80% after converting values from  $\log_{10}$  to the natural log. We fit a line to the data to determine the rate constant at 40 °C and RH of 80%.

#### ***Data for PEDV at pH values of 7.2, 9.2, and 10.2***

A 50% tissue culture infectious dose (TCID<sub>50</sub>) assay was reported in the work by Quist-Rybachuk, et al. We converted TCID<sub>50</sub> results to number of plaque forming units (PFU) by multiplying by 0.69 based on theory, as performed in prior work,<sup>29–31</sup> and then converted the data from  $\log_{10}$  to the natural log before calculating the slope based on the best fit lines that the authors provided in their plots. Data near the lower detection limit (LDL) had already been excluded from the authors' own analysis to avoid under-predicting the rate. The calculated slopes were used to determine the rate constants at 40, 44, and 48 °C for pH values of 7.2, 9.2, and 10.2, reported in **Table S1**.



## **S2. Processing of Virus Inactivation Data**

This section contains all of the raw values for the processed data included in **Figure 1**. The data points in **Figure 1(a)** are listed in **Table S1**, where the  $\ln(k)$  values were calculated from the  $k = -d(\ln([C]))/dt$  values determined in **Section S1**, unless otherwise noted in the table. The slope-intercept data for all of the linear fits in **Figure 1** are listed in **Table S2** and shown in **Figure S22**, along with the calculated activation energy and frequency factor shown in **Figure 1(b)**.

**Table S1.** Data plotted in **Figure 1(a)** in the main text.

Dataset	$T$ [°C]	$1/T \cdot 10^4$ [ $10^4/K$ ]	$k = -d(\ln([C]))/dt$ [1/min]	$\ln(k)$ [1/min]
SARS-CoV-1	56	30.40	0.9077	-0.0968
SARS-CoV-1	65	29.59	2.869	1.054
MERS-CoV	20	34.13	0.0027	-5.9145
MERS-CoV	56	30.40	0.16	-0.9985
MERS-CoV	65	29.59	3.62	2.1211
TGEV-D52	31	32.90	$\ln(k)$ provided in source	-7.963
TGEV-D52	35	32.47	$\ln(k)$ provided in source	-7.332
TGEV-D52	39	32.05	$\ln(k)$ provided in source	-6.439
TGEV-D52	43	31.65	$\ln(k)$ provided in source	-5.808
TGEV-D52	47	31.25	$\ln(k)$ provided in source	-4.837
TGEV-D52	51	30.86	$\ln(k)$ provided in source	-3.369
TGEV-D52	55	30.48	$\ln(k)$ provided in source	-1.823
TGEV-Purdue	31	32.90	$\ln(k)$ provided in source	-7.832
TGEV-Purdue	35	32.47	$\ln(k)$ provided in source	-7.149
TGEV-Purdue	39	32.05	$\ln(k)$ provided in source	-6.177
TGEV-Purdue	43	31.65	$\ln(k)$ provided in source	-5.468
TGEV-Purdue	47	31.25	$\ln(k)$ provided in source	-4.418
TGEV-Purdue	55	30.48	$\ln(k)$ provided in source	-1.849
TGEV-RH20	4	36.10	0.000042	-10.126
TGEV-RH20	20	34.13	0.00013	-9.21
TGEV-RH20	40	31.95	0.0014	-6.57

TGEV-RH50	4	36.10	0.000093	-9.316
TGEV-RH50	20	34.13	0.0014	-6.571
TGEV-RH50	40	31.95	0.0181	-4.012
TGEV-RH80	4	36.10	0.00017	-8.517
TGEV-RH80	20	34.13	0.00035	-7.824
TGEV-RH80	40	31.95	0.0115	-4.465
MHV-RH20	4	36.10	0.000012	-11.513
MHV-RH20	20	34.13	0.000095	-9.210
MHV-RH20	40	31.95	0.0018	-6.571
MHV-RH50	4	36.10	0.00017	-8.517
MHV-RH50	20	34.13	0.0016	-6.438
MHV-RH50	40	31.95	0.0114	-4.474
MHV-RH80	4	36.10	0.00013	-9.210
MHV-RH80	20	34.13	0.00080	-7.131
MHV-RH80	40	31.95	0.0113	-4.483
PEDV-pH 7.2	40	31.95	0.0211	-3.858
PEDV-pH 7.2	44	31.55	0.0326	-3.422
PEDV-pH 7.2	48	31.15	0.0900	-2.407
PEDV-pH 9.2	40	31.95	0.0863	-2.449
PEDV-pH 9.2	44	31.55	0.1295	-2.044
PEDV-pH 9.2	48	31.15	0.5178	-0.658
PEDV-pH 10.2	40	31.95	0.1618	-1.821
PEDV-pH 10.2	44	31.55	0.2728	-1.299
PEDV-pH 10.2	48	31.15	1.2943	0.258

598

599 **Table S2.** Slopes and intercepts of data plotted in **Figure 1(a)** in the main text, and the calculated  $\ln(A)$   
600 and  $E_a$  values shown in **Figure 1(b).**

Dataset	Slope [K/10 <sup>4</sup> ]	Intercept [1/min]	$E_a$ [J/mol]	$\ln(A)$ [1/min]
SARS-CoV-1	-1.4219	43.122	118223.876	43.122
MERS-CoV	-1.6282	49.48	135376.689	49.48
TGEV-D52	-2.4514	72.205	203821.653	72.205
TGEV-Purdue	-2.4717	73.094	205509.497	73.094

TGEV-RH20	-0.924	22.919	76825.98	22.919
TGEV-RH50	-1.2755	36.811	106051.448	36.811
TGEV-RH80	-0.9858	26.64	81964.341	26.64
MHV-RH20	-1.1905	31.449	98984.1225	31.449
MHV-RH50	-0.9724	26.644	80850.198	26.644
MHV-RH80	-1.1399	31.882	94776.9855	31.882
PEDV-pH7.2	-1.8196	54.177	151290.642	54.177
PEDV-pH9.2	-2.245	69.111	186660.525	69.111
PEDV-pH10.2	-2.606	81.262	216675.87	81.262

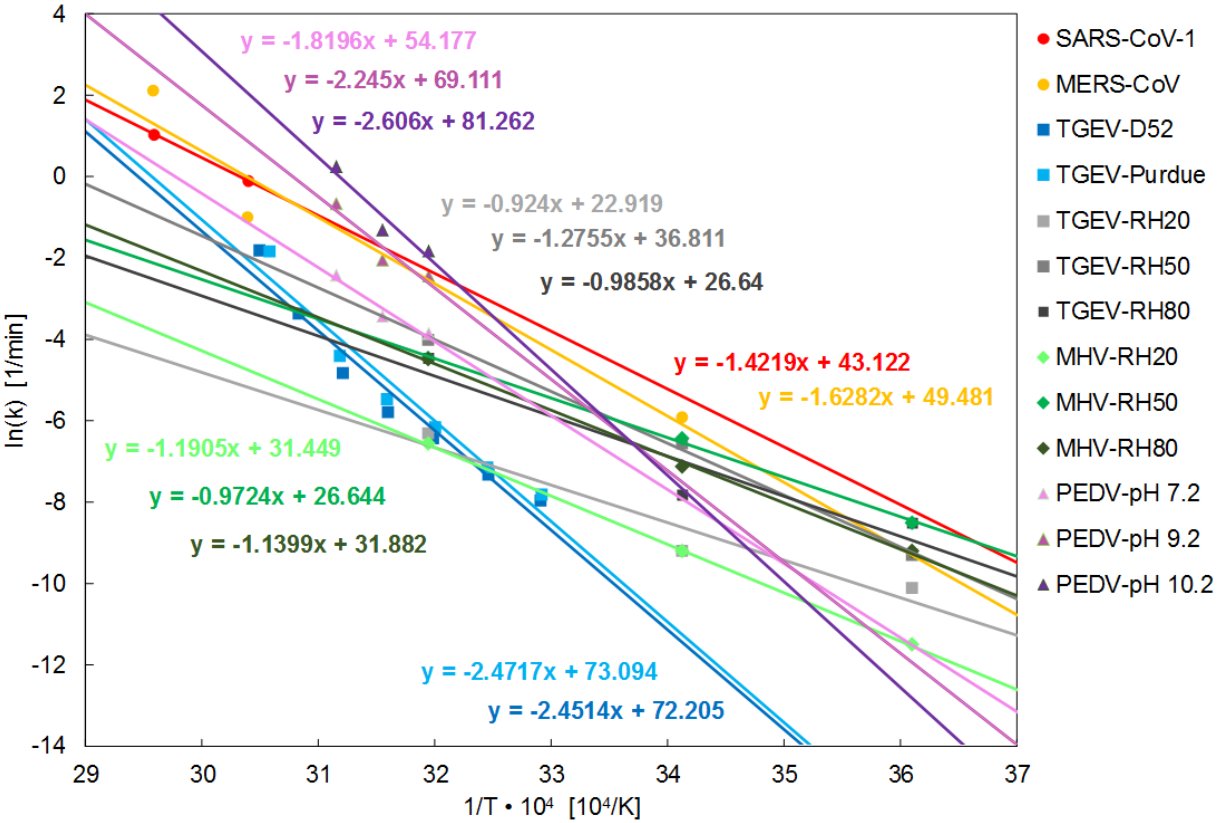


**Figure S22.** A magnified version of **Figure 1(a)** from the main text, with the slopes and intercepts for each linear fit indicated.

### **S3. Trends across Virus Strains, Relative Humidity, and pH**

Subsets of the model predictions for several viruses that varied only by strain, relative humidity, or pH of the surrounding medium are plotted here to more clearly highlight trends.

#### ***Trends across virus strains***

Comparing results for the TGEV-D52 and TGEV-Purdue strains, we did not observe any significant deviation in the model prediction between these strains, shown in **Figure S23**. We hypothesize that the similarity between these two strains may be indicative of a similarity that SARS-CoV-2 could exhibit with SARS-CoV-1; we have predictive capability for SARS-CoV-1 with the present model and data, and the predictions for SARS-CoV-1 may suggest the expected thermal degradation of SARS-CoV-2.

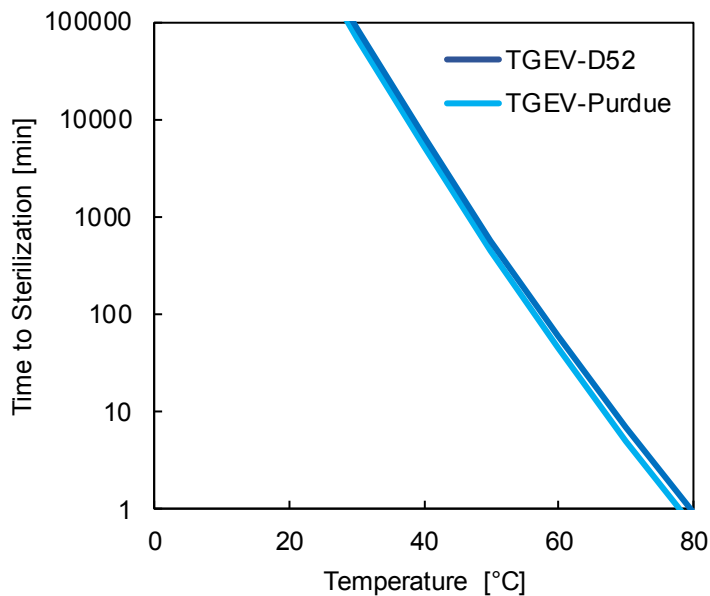


**Figure S23.** Model predictions for sterilization times required for the TGEV D52 and Purdue strains.

#### ***Trends across relative humidity conditions***

Comparing results for the TGEV and MHV viruses at relative humidity levels of 20%, 50%, and 80%, we did not observe any clear trends, as shown in **Figures S24** and **S25**. We note that the dataset obtained

from Casanova, et al., appeared to exhibit the most experimental error of all the data used in the model, especially at low temperatures, with  $R^2$  values as low as 0.1 when applying linear fits to several sets of their data in **Section S1**. Therefore, more data would be needed to rule out a correlation between virus inactivation and relative humidity, especially considering such a trend has been implied in prior work.<sup>43</sup>

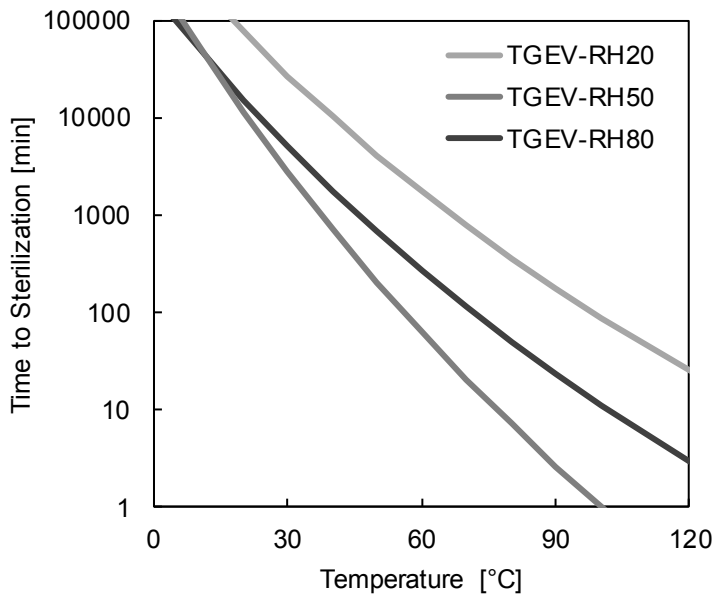


**Figure S24.** Model predictions for sterilization times required for TGEV at levels of relative humidity of 20%, 50%, and 80%.

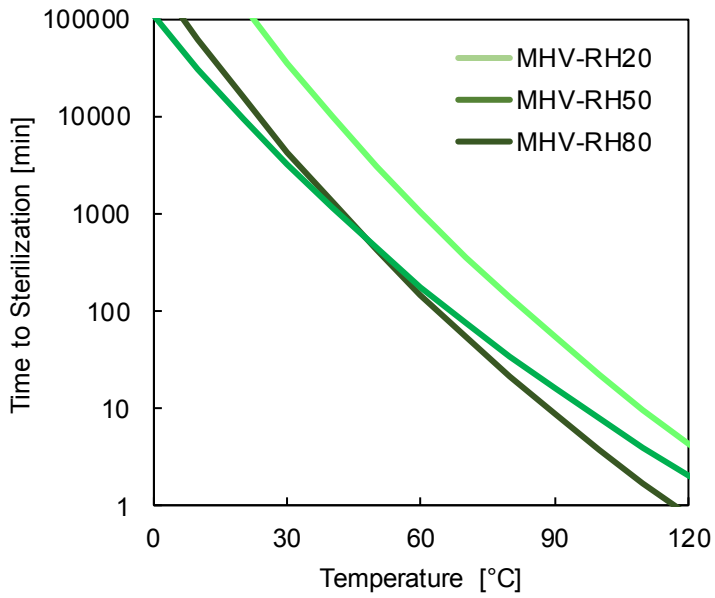


**Figure S25.** Model predictions for sterilization times required for MHV at levels of relative humidity of 20%, 50%, and 80%.

#### ***Trends across pH levels***

Comparing results for PEDV across pH levels of 7.2, 9.2, and 10.2, we observed a faster rate of virus inactivation at more basic pH levels as reported in prior work,<sup>27</sup> shown here in **Figure S26**.

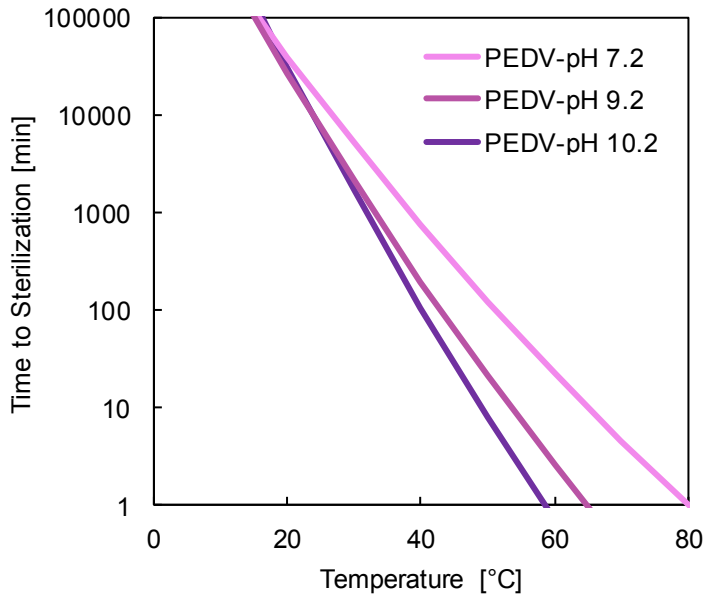
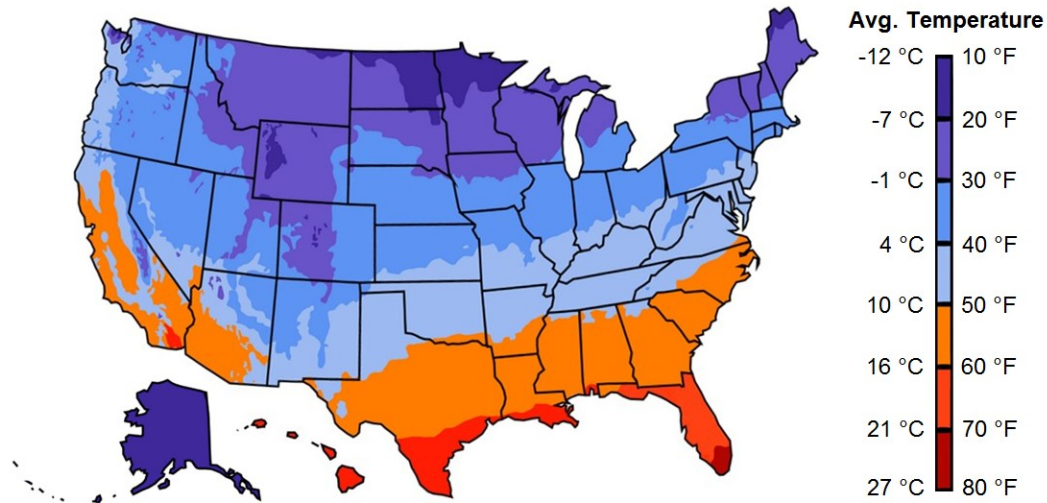


**Figure S26.** Model predictions for sterilization times required for PEDV at pH levels of 7.2, 9.2, and 10.2.

#### **S4. Conversion of Climate Data to Inactivation Timescale Map**

The national average temperature map of the United States for the months of January to March, 2020, was obtained from the National Oceanic and Atmospheric Administration (NOAA). This temperature map, shown in **Figure S27**, displays the CONUS mean temperature (except data for Hawaii and Alaska, which were obtained from NOAA's climate data online search). The average temperature values encompassing January through March, 2020, were chosen in accordance with the timeline of the COVID-19 pandemic to date.



652

653 **Figure S27.** Initial data from NOAA used to generate **Figure 3** in the main text; average temperatures

654 over the period encompassing January to March, 2020, are shown.